

Section headings : Cavity and void detection

SOIL CRACKS DETECTION BY 3D ELECTRICAL RESISTIVITY

Samouëlian, A.¹, Cousin, I.¹, Richard, G.², Bruand, A., ⁴Tabbagh, A.³

(1) INRA, Unité de Science du Sol, BP 20619, 45166 Ardon France

(2) INRA Unité d'Agronomie, rue Fernand Christ, 02007 Laon France

(3) UMR 7619 « Sisyphe », Case 105, 4 place Jussieu, 75005 Paris

(4) UMR 6113 ISTO, 1a rue de la fêrolierie, 45071 Orléans Cedex 2

Introduction

Soil cracks, whose formation are associated to natural climate phenomena such as swelling and shrinking, play an important role in water and gas transfers. Up to now, their 3D structure was characterised either by serial sections (Cousin, 1996) which is a destructive technique or X-ray tomography (Macedo et al., 1998) which is applicable on limited size sample. Three-dimensional electrical resistivity prospecting enables now to monitor crack development and to characterise their geometry without any destruction of the medium under study. Three-dimensional electrical resistivity surveys are commonly gathered by a network of in-line survey arrays, such as Wenner, Schlumberg, or dipole-dipole (Xu and Noel, 1993; Zhou et al., 2002). As emphasized by Meheni et al. (1996) the resulting apparent resistivity maps are often different depending on the array orientation related to an electrical discontinuity. Chambers et al. (2002) underline that in heterogeneous medium 3D electrical resistivity model resolution was sensitive to electrode configuration orientation. Indeed asymmetric bodies or anisotropic material exhibit different behaviours depending on whether the current passes through them in one direction or in another (Scollar et al., 1990). It would be all the more true for medium having very contrasted resistivities like cracking soil. In that case the electrical current does not encounter the same resistance when it passes perpendicular or parallel to the resistant bodies. Measurements of apparent resistivity depend then on the location and orientation of the current source relative to the body under study (Bibby, 1986). Studies conducted by Habberjam and Watkins (1967) emphasized that the square array provide a measurement of resistivity less orientationally dependent than that given by a in-line array investigation.

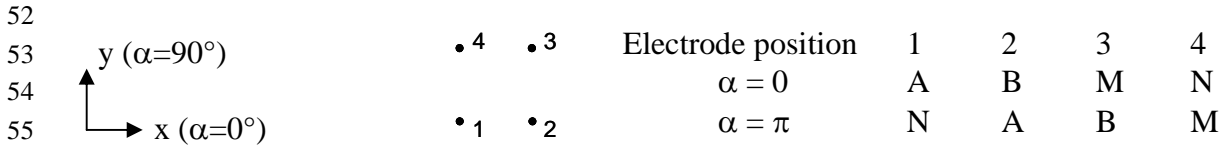
Intending to lead a more 3D accurate inversion, we have chosen to focus our attention on a 3D electrical resistivity data acquisition. We present here a three-dimensional electrical survey carried out by a square array quadripole for characterising the soil cracks network developing during a desiccation period.

Material and Method

The experiment was conducted on a loess soil block (26 by 30 by 40 cm³ in size). It exhibited a massive structure resulting from severe compaction after wheels traffic in wet conditions. At sampling, the initial volumetric water content was 0.43 cm³cm⁻³. It was then let to dry for 18 days. During this time, the soil porosity increased: cracks appeared at the soil surface and spread toward the soil at depth.

The electrical resistivity measurements were done by 64 Cu/CuSO₄ electrodes arranged on 8 lines by 8 columns as shown in fig.1. The electrode spacing "a" was chosen equal to 3 cm, which was a priori supposed to achieve the detection of millimetre cracks as shown in a previous experiment at the centimetre scale (Samouëlian et al., 2003). The number of data was 280 measurements spread out 7 pseudo-depths. For each array, 2 measurements were done, the current being injected in 2 perpendicular directions. The respective apparent

50 electrical resistivity measurements were noted ρ_{0° and ρ_{90° , if ρ_{0° and ρ_{90° are equal, the
 51 sounding medium is homogenous with no electrical heterogeneity.



56 Figure 1 : Square array configuration and possible modes of connection

57

58 **Results and discussion**

59 Global description of the 3D apparent resistivity data at the end of the experiment

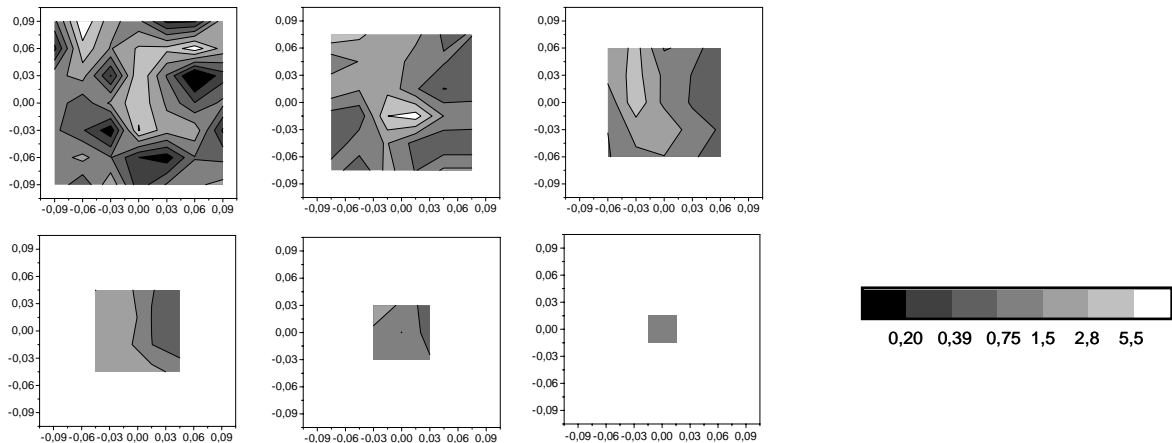
60 Resulting from the two-array orientation $\alpha=0^\circ$ and $\alpha=90^\circ$, we calculated an apparent
 61 anisotropic index (*AI*) defined by equation [1] :

$$AI = \frac{\rho_{0^\circ}}{\rho_{90^\circ}} \quad [1]$$

62

63 The determination of electrical anisotropy index was suitable as it may enhance the presence
 64 of heterogeneities. It permitted also to summarize for each pseudo-depth the electrical
 65 resistivity measurements on a single map (figure 2). The *AI* revealed major anisotropic zones
 66 linked to elevated or low *AI* values. As expected, they were rather located at the soil surface
 67 than at depth: the apparent anisotropic index varied from 0.07 to 9.63 in the first pseudo-
 68 depth, in the second and third pseudo depths the variation decreased slightly 0.38 to 0.5 for
 69 the minimum values and 7.54 to 4.64 for the maximum values. The deeper pseudo-depths,
 70 four, five, and six, did not exhibit large variations, because the size of the array was probably
 71 larger than the crack extents.

72



73

74

75

76

77

78

79

80

81

82

83

84

85 Figure 2 : Spatial distribution of the Anisotropic Index (*AI*) at the final stage

86

87 Cracks detection for the first pseudo-depth

88 *AI* can be considered as an indicator of cracks detection. For the first pseudo-depth, we
 89 determined the relation between *AI*, the mean crack width and the crack orientation for each
 90 elementary area. When the crack width was greater than 1 mm, two groups could be
 91 distinguished related to the thresholds I_{cinf} and I_{csup} corresponding respectively to 0.42 and
 92 to 3.14. When the relation $I_{cinf} < AI < I_{csup}$ was verified, the related zone was considered as a
 93 no cracking zone; when it was not verified, the related zone was considered as a cracking
 94 zone (figure 3). The crack preferential orientation ($\alpha = 0^\circ$ or $\alpha = 90^\circ$) could also be deduce by
 95 the *AI* value. When it was larger (resp. smaller) than 1, the preferential orientation was $\alpha =$
 96 90° (resp. 0°). Moreover one can notice that cracks that do not cross the MN in-line
 97 measurements have an *AI* value between I_{cinf} and I_{csup} .

98

99 Figure 3 : Crack detection and orientation for the first pseudo-depth evaluated by
 100 the *AI* The white represented the no-cracking area, the grey and light grey



101 represented the cracking area, respectively with cracks preferential orientation 0° and 90°

102 Cracks detection of the all the pseudo-depth

103 a) Calculation of a new index

104 The apparent anisotropy index, AI , presented previously can be used as an indicator of
 105 discontinuities like cracks yielding both position and orientation. Nevertheless it is directly
 106 calculated by the mean experimental data and as a consequence, the thresholds values given in
 107 this paper cannot be generalized to another dataset that would be obtained either on another
 108 soil or in different experimental conditions. Thus, we have calculated a second index. To look
 109 for the preferential anisotropic orientation, we searched the α -array orientation corresponding
 110 to the maximum apparent resistivity values also called α_{\max} -array orientation. The primary
 111 data set was transformed into a calculated data set with the help of the rotational tensor R
 112 expressed in the equation [2].

$$113 \quad R = \begin{pmatrix} \cos \alpha & \sin \alpha \\ -\sin \alpha & \cos \alpha \end{pmatrix} \quad [2]$$

114 Thus a calculated data set was obtained by the equation [3] :

$$115 \quad \begin{pmatrix} \rho_\alpha \\ \rho_{\alpha+90^\circ} \end{pmatrix} = |R| \begin{pmatrix} \rho_{0^\circ} \\ \rho_{90^\circ} \end{pmatrix} \quad [3]$$

116 where : ρ_α and $\rho_{\alpha+90^\circ}$ were the calculated data set obtained for α value varying by 5° steps
 117 between 0° and 90° . The rotational tensor highlighted particular features such as the position
 118 and orientation of a resistivity discontinuity.

119 b) Calculation of the α_{\max} values on the experimental dataset

120 As summarized in table [1], the distance between the minimum and maximum values of the
 121 α_{\max} -array orientation decreased as the pseudo-depth increased. Moreover the values were
 122 converging to $\alpha=45^\circ$, corresponding to a medium without electrical heterogeneities.
 123

	PP1	PP2	PP3	PP4	PP5	PP6
Mini	5	10	10	20	35	45
Max	85	70	65	65	65	50

124 Table 1 Extremes values of α_{\max} -array orientation.

125 The figure 4 exhibits the spatial distribution of the α_{\max} . For the first pseudo-depth, the α
 126 values ranging between 40 and 50 corresponded to the elementary area where $I_{cinf} < AI$
 127 $< I_{csup}$. They were associated with an isotropic medium. The α values ranging in the interval
 128 0-35 and 55-90 were associated with an anisotropic medium, corresponding to the cracks
 129 network. Between the first and the second pseudo-depths, the electrical heterogeneities
 130 orientation were preserved or shifted to 45° but never inverted. Depending on the quadripole
 131 position the cracks larger than 1mm were detected. Cracks spread out the soil depth with a
 132 preferential orientation initiated from the surface. One can also supposed that as the mean
 133 crack width increased the corresponding crack depth increased too. For the third pseudo-depth
 134 we focused only on the crack mean width larger than 1 mm. Only the triple point was then
 135 partially recorded. The crack oriented at 90° was the best detected. As observed at the soil
 136 surface, the mean width of this crack nevertheless was the highest: 2.57 mm. The following
 137 pseudo-depths four, five, and six displayed an orientation α converging to 45° .

138 In summarize, the studied soil depth does not exhibit any electrical anisotropy and the
 139 cracking zone was mainly located at the surface. With an inter-electrode spacing of 3cm,
 140 cracks of 1mm width were detected at the soil surface. When the inter-electrode spacing
 141 increased from a to 2a (second pseudo-depth), only the major cracks were distinguished. The
 142 widest cracks were detected until the third pseudo-depth. As the pseudo-depth increased, the

sounding soil volume increased too and the related influence of cracks decreased. The electrical signal became then less disturbed by the heterogeneities

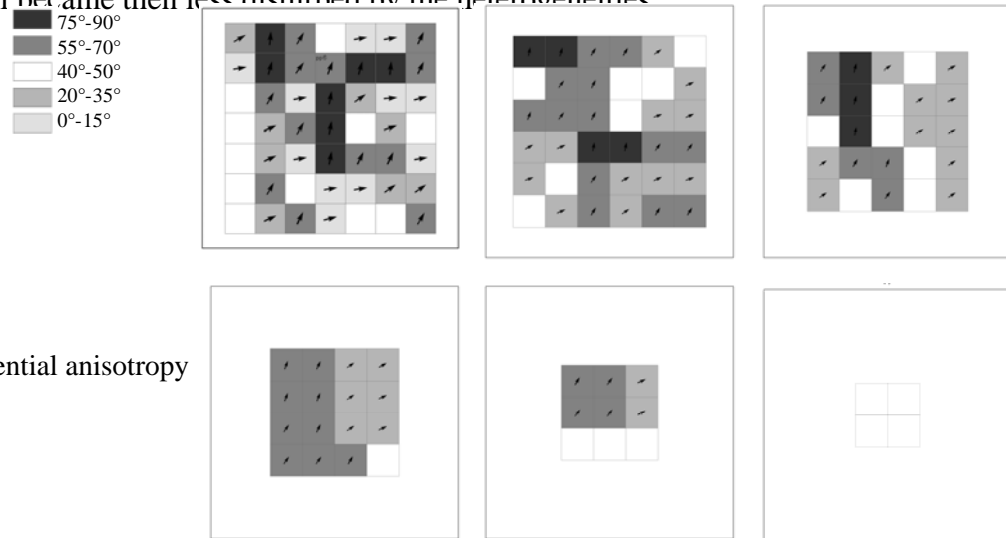


Figure 4: Preferential anisotropy orientations

Conclusion

These results indicated that electrical resistivity measurement was as expected dependent on the electrical heterogeneities and the variation of signal was even detectable at this scale. The I_{cinf} and I_{csup} thresholds resulting of the anisotropic index AI and the α_{max} -array orientation are two methods useful for detecting electrical heterogeneities. The first one was calculated for a specific electrical device, related to a specific soil texture and experimental condition. Nevertheless they can be applied to electrical acquisition corresponding to the temporal monitoring of the desiccation experiment. The second method required time for calculation but presented the advantage to be generalisable to the whole soil volume. The calculation of these 2 indexes gives ideas on the structure of the medium prior to the data inversion. Nevertheless for the both method, cracks oriented near $\alpha=45^\circ$ or cracks who do not cross the in-line measurement MN were not detected. One suggestion is to collect the electrical measurement for in-line measurement along diagonal, which would also increase the acquisition time of about 20 min.

References :

- Bibby, H. M. 1986. Analysis of multiple-source bipole-quadrupole resistivity surveys using the apparent resistivity tensor. *Geophysics* 51: 972-983.
- Chambers, J. E., R. D. Oglivy, O. Kuras, J. C. Cripps and P. I. Meldrum. 2002. 3D electrical imaging of known targets at a controlled environmental test site. *Environmental Geology* 41: 690-704.
- Cousin, I. 1996. Reconstruction 3D par coupes s eriees et transport de gaz dans un milieu poreux. Application   l' tude d'un sol argilo-limoneux, Reconstruction 3D par coupes s eriees et transport de gaz dans un milieu poreux. Application   l' tude d'un sol argilo-limoneux. Universit  d'Orl ans.
- Habberjam, G. M. and G. E. Watkins. 1967. The use of a square configuration in resistivity prospecting. *Geophysical Prospecting* 15: 445-467.
- Macedo, A., S. Crestana and C. M. P. Vaz. 1998. X-ray microtomography to investigate thin layers of soil clod. *Soil & Tillage Research* 49: 249-253.
- Meheni, Y., R. Gu rin, Y. Benderitter and A. Tabbagh. 1996. Subsurface DC resistivity mapping : approximate 1-D interpretation. *Journal of Applied Geophysics* 34: 255-270.
- Samou lian, A., I. Cousin, G. Richard, A. Tabbagh and A. Bruand. 2003. Electrical resistivity imaging for detecting soil cracking at the centimetric scale. *Soil Science Society Journal of America*.in press
- Scollar, I., A. Tabbagh, A. Hesse and I. Herzog. 1990. Archaeological prospecting and remote sensing.
- Xu, B. and M. Noel. 1993. On the completeness of data sets with multielectrode systems for electrical resistivity survey. *Geophysical Prospecting* 41: 791-801.

195 Zhou, Q. Y., J. Shimada and A. Sato. 2002. Temporal variations of the three-dimensional rainfall infiltration
196 process in heterogeneous soil. *Water Resources Research* 38: 1-16.
197